DOI: 10.13009/EUCASS2017-159

Optical Analysis of the Liquid Layer Combustion of Paraffin-based Hybrid Rocket Fuels

Anna Petrarolo⋆†*, Mario Kobald*⋆ *and Stefan Schlechtriem*⋆
⋆ *DLR, German Aerospace Center, Institute of Space Propulsion*
Langer Grund, 74239 Hardthausen, Germany
anna.petrarolo@dlr.de · mario.kobald@dlr.de
† Corresponding Author

Abstract

The combustion behaviour of paraffin-based hybrid rocket fuels in combination with gaseous oxygen (GOX) was investigated in the framework of this research. Tests were performed in a 2D slab burner configuration with windows on two sides at atmospheric conditions. High speed videos were recorded and analysed in detail by using an automated video evaluation routine. Two different decomposition techniques were applied to the scalar field of the flame luminosity. The results show that the combustion is dominated by wave-like structures and that the most excited frequencies and wavelengths characterizing the liquid melt layer depend on the fuel viscosity and geometry.

1. Introduction

1.1 Hybrid Rocket Engines

Hybrid rocket engines (HRE) typically consist of a solid fuel and a liquid or gaseous oxidizer. Due to the fact that the propellants are stored in two different states of matter, HRE have some advantages compared to classical solid or liquid rocket engines. Considering storage and handling, they are safer than solid motors. This also contributes to reduce the total cost of the engine. Moreover, they are characterized by controllable thrust, including shut off and restart capability. With respect to liquid engines, they are mechanically simpler and, consequently, cheaper.[28] However HRE are historically characterized by low regression rate and combustion efficiency, due to the use of polymeric fuels, such as Hydroxyl-terminated Polybutadiene (HTPB) or High-Density Polyethylene (HDPE). In fact, the regression rate of classical polymeric hybrid fuels is diffusion limited and hindered by the blocking effect. In a HRE the combustion occurs in the turbulent boundary layer over the fuel surface and the flame is located where there is a combustible ratio between the vaporized oxidizer and fuel.[43] The heat is then radiated and convected from the diffusion flame to the fuel surface. In a classical hybrid, the polymeric fuel pyrolyses and its vapours are transported to the diffusion flame where it reacts with the atomized oxidizer transported from the free stream via turbulent diffusion.[11] The problem of the low performance of HRE was overcome in the past by increasing the fuel burning area with the use of multi-port fuel grains, which, on the other hand, increase the complexity of the system and the residual mass of unburned fuel (which leads to a decrease in the delivered specific impulse).

Recently, a new class of high regression rate hybrid rocket fuels has been discovered: they are characterized by low viscosity and surface tension.[26] Cryogenic solid n-pentane showed regression rates 5-10 times higher than polymeric hybrid fuels.[7,38,39] Paraffin-based fuels, tested at Stanford University, show a 3-5 times higher regression rate at similar mass fluxes compared to polymers.[23,24] This is achieved by a different combustion mechanism. Paraffin fuels form a thin liquid layer on the fuel surface during the combustion.[24] It is expected that the low viscosity and surface tension of the liquid fuel enable an additional mass transfer by entrainment of liquid droplets. The gas flow over the surface induces liquid layer instabilities which produce the droplet entrainment,[25] see also Fig. 1. The entrainment mechanism works like a spray injection along the length of the motor, which increases the effective fuel burning area and reduces the blocking effect. This enables simple, single-port fuel grain designs and makes hybrid propulsion a competitive candidate for launch systems and in-space missions.

DOI: 10.13009/EUCASS2017-159

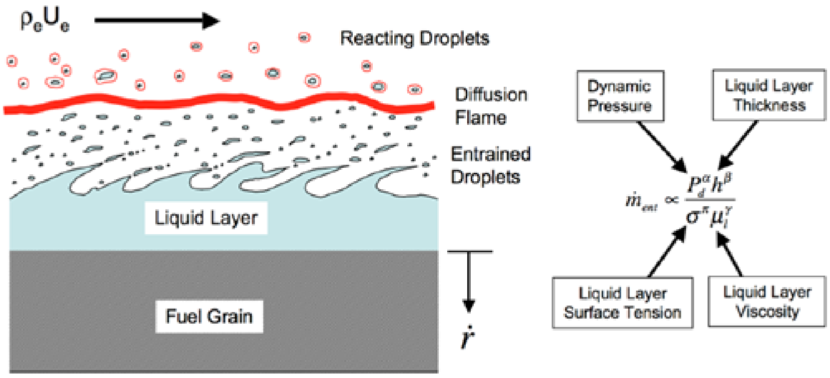

Figure 1: Liquefying fuel combustion theory, taken from Karabeyoglu et al.[22,27]

Optical results of the entrainment process of low viscosity liquefying fuels are shown in Fig. 2. Scale-up tests were done and confirmed that the theory is applicable also for engines at larger scale.[29] Recent tests with different paraffin-based fuels and gaseous oxygen (GOX) showed an exponential relation between the liquid layer viscosity and the overall regression rate,[34] which proves the predicted entrainment correlation in Fig.1.

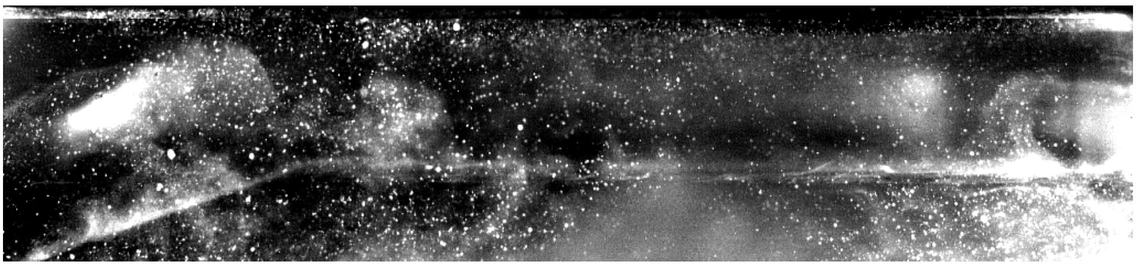

Figure 2: Liquefying fuel combustion image created within this research (oxidizer mass flow from left to right)

1.2 Optical Investigations of Hybrid Rocket Combustion

The discovery of liquefying hybrid rocket fuels has renewed the interest in hybrid propulsion and in optical investigations of the hybrid rocket combustion process. The theory of the Kelvin-Helmholtz instability (KHI) and of the liquid layer break up process, which leads to the fuel droplet entrainment, are well explained in the literature.[1,15,24,25] The increase in regression rate is proven at different thrust levels[29,52] and some detailed optical investigations have been performed in the recent years in order to capture the entrainment process. Some of them are described herein.

In 2009, Pelletier investigated the combustion behaviour of paraffin-based fuels, but no further correlations have been found between the theory and the experiments.[45] In 2011, Nakagawa et al. investigated the dependence of the regression rate on the fuel viscosity. They performed optical tests at atmospheric pressure with different paraffin-based fuels and gaseous oxygen. Their images showed that droplets are generated during the combustion and entrained in the flow.[44] De Luca et al. also used an optical technique to investigate the hybrid combustion process. They looked inside a pressurized chamber over a mirror set-up and thereby measured the instantaneous regression rate.[13] Many optical investigations on the combustion behaviour of both polymeric and paraffin-based hybrid rocket fuels have been done at the Stanford Combustion Visualization facility. In 2012, Chandler et al. investigated the combustion of paraffin-based fuels with gaseous oxygen at both atmospheric and elevated pressures. Their results showed roll waves and droplets in the atmospheric tests and filament-like structures along the sides of the fuel grains in the tests run at elevated pressures.[8] Moreover, they compared the combustion behaviour of paraffin-based fuels to that of classical hybrid fuels. They reported that for paraffin-based fuels entraining droplets were visible, for HDPE (High Density PolyEthylene) only little droplet entrainment was seen and for HTPB (Hydroxyl-Terminated PolyButadiene) no droplet entrainment was measured.[9] In 2014-2016, many optical tests were conducted from Jens et al. with the same facility. They performed Schlieren and OH* images of the combustion of different classical polymeric and paraffin-based fuels in combination with gaseous oxygen at both atmospheric and elevated pressures.[19] They reported unsteady blowing events of paraffin droplets in the tests at higher pressure, slightly above the critical pressure of their paraffin samples. Schlieren results

DOI: 10.13009/EUCASS2017-159

of their tests reported a thickening boundary layer with increasing pressure.[18] Tests at atmospheric pressure were conducted also with HTPB, HDPE and PMMA (PolyMethyl MethAcrylate). No drastic change in boundary layer thickness growth was observed between paraffin wax and classical polymeric fuels.[21] On the other hand, the flame zone of the paraffin wax was found to be much thicker than that of the classical fuels.[20] In 2014, Wada et al. visualized the combustion of different polymeric fuels and paraffin. The investigated pressure range was from 1 up to 20 bar. In contrast to the other mentioned optical experiments, this set-up looks at the combustion of opposing slabs of fuel mounted vertically. From their observations, they concluded that both the number and size of the entrained droplets are independent of the chamber pressure.[51] Tada et al. investigated the effect of swirling oxidizer injection with paraffin fuel. Tests were done at elevated pressures. The optical access for the camera was provided from the injector side in order to investigate the flame behaviour for different swirl injection patterns.[50] Many optical investigations have also been done at the German Aerospace Center (DLR) since 2013. Kobald et al. performed visual and Schlieren images of the combustion of paraffin wax and gaseous oxygen at atmospheric pressure. They reported visualization of droplets entrainment during start-up and shut-down transients.[31,33] Since 2015, an automated video evaluation routine has been developed in DLR, in order to capture the dominant flow dynamic and combustion behaviour of paraffin-based hybrid rocket fuels during a typical test.[32,37,46,47] The latest results of this research are presented in this paper.

2. Theoretical Background: Decomposition Methods

2.1 Proper Orthogonal Decomposition

The POD (Proper Orthogonal Decomposition) has been used in diverse area of research to obtain approximate, low-dimensional descriptions of turbulent fluid flows, structural vibrations and dynamical systems. It has also been extensively used in image processing, signal analysis and data compression.[10]

The POD is a statistical method where an orthogonal transformation is used to convert a set of data into a set of linearly uncorrelated variables, which are called principal components. Their number is usually less than the number of the original variables. This transformation is performed so that the principal components are sorted by decreasing variance under the constraint that each component has to be orthogonal to the preceding ones, thereby being uncorrelated. An orthogonal transformation to the basis of the eigenvectors of the sample covariance matrix is performed and the data are projected onto the subspace spanned by the eigenvectors corresponding to the largest eigenvalues (most energetic modes). So, POD gives an orthogonal basis that ranks modes according to an energy criterion.[5] This enables us to retain only the dominant modes and to filter out the presence of the measurement noise, thus providing a good characterization of the dynamics of the problem. Finally, POD is able to explicitly separate the spatial and time information.[30] On the other hand, the linear nature of the method can be a restriction for some data sets. Moreover, since POD removes linear correlations among variables (i.e. diagonalizes the covariance matrix), it is only sensitive to second-order statics. This means that this method is able to find only uncorrelated variables.[30]

In the present work, the POD is applied to the analysis of the luminosity field of images (scalar field) in a reactive flow. This allows for an analysis of the considered scalar field by decomposing it into mean, coherent and incoherent parts via statistical methods and to visualize the relevant morphologies. In general, the coherent part includes all fluctuations possessing a somehow structured feature over the burning process. The incoherent part includes all fluctuations for which no pattern can be identified over the burning process. It is commonly thought that the first few modes correspond to the average structure of the data, while higher order modes contain information about fluctuations.[3] The Nonlinear Iterative Partial Least Squares (NIPALS) algorithm is used for the principal component analysis in the POD method. The Power Spectral Density (PSD) of the temporal and spatial coefficients is performed at the end of the algorithm in order to obtain the excited frequencies and wavelengths during the combustion.

2.2 Independent Component Analysis

The ICA (Independent Component Analysis) is a statistical signal processing technique whose main applications are blind source separation, blind deconvolution and feature extraction.[16] One application with combustion was demonstrated by Bizon et al.[2,4] They applied ICA to 2D images of combustion-related luminosity, in order to identify leading independent structures.

The ICA is a statistical and computational technique for revealing hidden components that underlie the observed data. The latent variables are assumed to be non-Gaussian and mutually independent in space and/or time: they are called the independent components of the observed data. The transformed variables correspond to the underlying components that describe the essential structure of the data and that correspond to some physical causes involved in

DOI: 10.13009/EUCASS2017-159

the process. The method which is used in this analysis for finding the independent components is the maximization of non-Gaussianity of the sample matrix.[17] Each local maximum or minimum gives one independent component.

The ICA is a much more powerful method with respect to the POD. The basis functions found by the POD, which reflect the directions of the most prominent variances in the data, are uncorrelated but not statistically independent. This means that higher order dependencies still exist and, therefore, they are not properly separated. In other words, all POD modes contain some element of all structures found in all of the fields.[4] On the other hand, ICA is able to search for basis functions that are statistically independent or as independent as possible, increasing the independence to higher statistical orders. When deriving these components, the data are separated into either spatially (sICA) or temporally (tICA) independent components; each choice yields corresponding statistically independent images or time courses. In particular, tICA produces a set of mutually independent temporal sequences and a corresponding set of unconstrained images. sICA determines mutually independent images and a corresponding set of unconstrained temporal sequences,[2,14] see also Fig. 3.

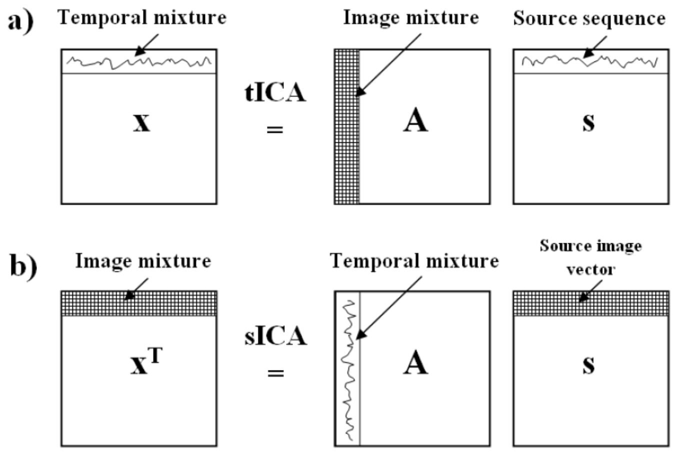

Figure 3: Vector Matrix representation of the mixing process for tICA and sICA, taken from Stone[49]

Some weak points have to be highlighted also for ICA: unlike for the principal components of the data, which are ordered according to their variance, no intrinsic order exists for the independent components. Moreover, ICA provides a solution only up to a multiplicative constant. In other words, the order, the signs and the scaling of the independent components cannot be determined: indeterminacy is an inherent property of this analysis.[17]

The aim of the present work is to identify independent spatial structures evolving in time. Therefore, the spatial ICA is applied to the analysis of the luminosity field of the combustion process in a hybrid engine. This allows the identification of the leading independent structures during the burning process. The FastICA algorithm[17] is employed. It maximizes non-gaussianity by means of a gradient method, estimated by the absolute value of kurtosis, as a measure of statistical independence. The Power Spectral Density (PSD) of the temporal and spatial coefficients is performed at the end of the algorithm in order to obtain the excited frequencies and wavelengths during the combustion.

3. Experimental Set-Up and Methods

3.1 Paraffin Fuels

Four different paraffin-based fuels have been investigated in the framework of this research. The wax that has been used as a base for all the fuels is type 6805 from the manufacturer Sasol Wax. It has been chosen because of its viscosity and surface tension values, which are the two fuel parameters that are expected to have the biggest influence on the entrainment process (see also Fig. 1). Detailed laboratory experiments have been performed before, in order to measure these two parameters for the different fuels.[34,36] All samples for the ballistic tests have been blackened by additives during fabrication to limit radiation effects during combustion to the fuel surface. Generally, the amount of blackening additive was less than 2% and has therefore negligible impact on the performance. Three different percentages of a commonly available polymer have also been added to the paraffin samples, in order to have different viscosity values. In this way it was possible to study the influence of this parameter on the entrainment process.

Moreover, three different fuel configurations have been investigated. Combustion tests with fuel slabs with 5°, 20°and 90°forward facing ramp angle have been performed (see Fig. 4) and the influence of the fuel configurations on

DOI: 10.13009/EUCASS2017-159

the combustion and entrainment process has been investigated.

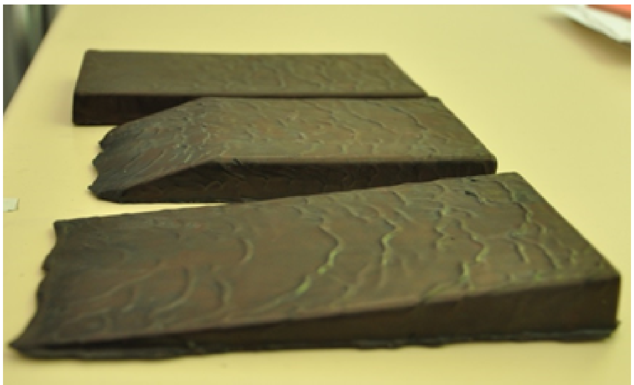

Figure 4: Different fuel configurations used in this research

3.2 Test Set-Up and Data Acquisition

The experimental tests were performed at the Institute of Space Propulsion at the DLR Lampoldshausen at the test complex M11. An already existing modular combustion chamber, used in the past to investigate the combustion behaviour of solid fuel ramjets, was adjusted and used for the test campaigns.[12] With this set-up, it is possible to perform tests both with and without a facing step placed before the fuel grain, which provides adequate flame holding and assures combustion stability. Tests performed in the framework of this research were all done without the flame holding step. A side view of the whole combustion chamber set-up is shown in Fig. 5. The oxidizer main flow is entering the combustion chamber from the left, after having passed two flow straighteners. Its mass flow rate is adjusted by a flow control valve and it is measured with a Coriolis flow meter with an accuracy better than 0.35% and a repeatability better than 0.2% of the flow rate. Ignition is done via an oxygen/hydrogen torch igniter from the bottom of the chamber. The two windows at each side enable several different optical diagnostic tools already used in the past, such as a color Schlieren setup, Particle image velocimetry (PIV), coherent anti-stokes Raman spectroscopy (CARS) and a gas sampling probe system. A test sequence is programmed before the test and is run automatically by the test bench control system. More details about the test bench and test settings are given in Kobald et al. and Petrarolo et al.[31,32,35,46]

In the framework of this research, all tests were done at atmospheric pressure and with an oxidizer mass flow ranging from 10 to 120 g/s. Combustion tests were performed using a single-slab paraffin-based fuel in combination with gaseous oxygen. Three fuel slab configurations with different forward facing ramp angle were tested. Burning time was 3 seconds for each test. For video data acquisition a Photron Fastcam SA 1.1 high speed video camera was used with a maximum resolution of 1024x1024 pixel. The frame rate, resolution and shutter time of the camera were adjusted for each test, according to the test conditions and position of the camera.

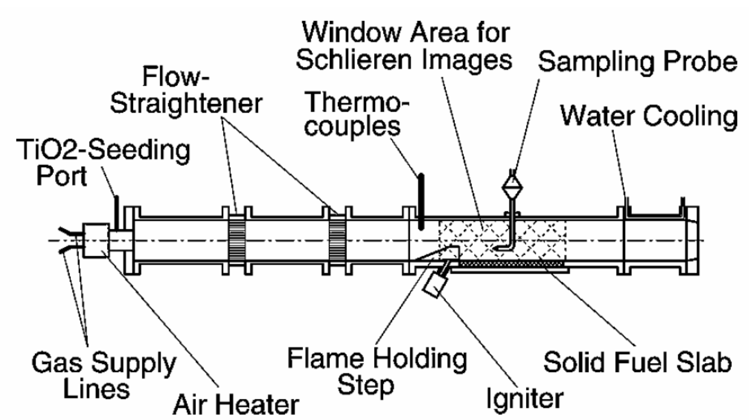

Figure 5: Sideview of the combustion chamber set-up

DOI: 10.13009/EUCASS2017-159

3.3 Video Analysis

The combustion high-speed videos are analysed with a Matlab®routine, which returns as results the most excited frequencies and wavelengths characterizing the liquid melt layer.

As first step, a video pre-processing is performed, see Fig.6. During this phase, the images are exported from the video and cropped with the Software VirtualDub. Usually filters are added, to adjust the brightness and the contrast of the images. The function sharpen is also used to enhance the contrast of adjacent elements. There exists also lateral burning at the sides of the fuel, so the bottom of the fuel is cropped just up to the solid liquid interface, to reduce noise and errors. Yet, the size of the area of interest is kept as large as possible in order to capture the flow dynamics on the whole upper surface of the fuel slab. The angled front and the rear end, where further vortices are created, are not included in the frames. The images are then exported to Matlab®and converted from true-color RGB to binary data images, based on a luminance threshold. The background noise, which usually consists of small light spots (most likely burning paraffin droplets), is removed. Finally, the waves edge is automatically detected and a sparse matrix is created. Each frame is then rearranged as a column vector and the Snapshot Matrix, which contains all the frames to analyse, is created. It has to be noticed that the recorded video data is a line of sight measurement. Thus, the data in the analysis represent an integrated measurement over the whole fuel slab width. This has to be taken into account when they are analysed. In a second step, the Snapshot Matrix is decomposed with both algorithms, POD and ICA, into two matrices containing spatial and temporal coefficients. At the end, the Power Spectral Density (PSD) of these coefficients is performed, in order to obtain the most excited frequencies and wavelengths during the combustion. Further details of the applied methods are given in Kobald et al.[37] and Petrarolo et al.[46]

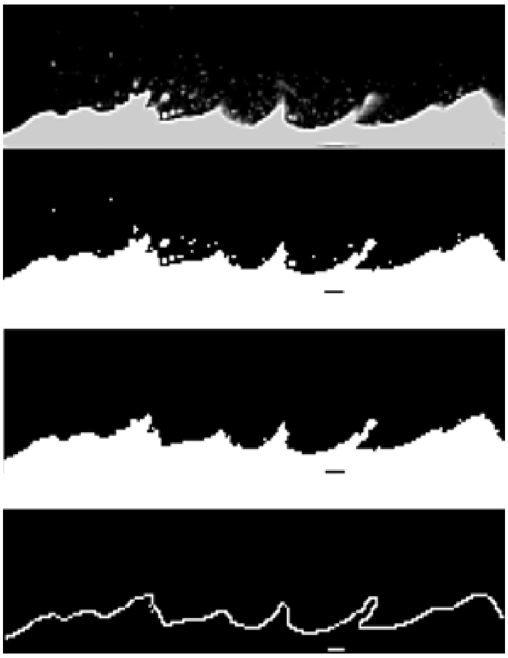

Figure 6: Video data pre-processing steps

4. Viscosity Measurements

Viscosity measurements of the paraffin samples are necessary for determining how this parameter influences the entrainment process. Analytical formula for material properties like surface tension and viscosity of paraffin waxes are available in different publications (e.g. Marano and Holder[40–42]). Unfortunately, these are often only valid for straight paraffin with distinct carbon numbers. Therefore, they cannot be applied for most of our samples, as well as for paraffin-based mixtures.

Viscosity measurements of the four kind of paraffin-based fuels used in this research were performed in the M3 chemical laboratory at the DLR Lampoldshausen. Early viscosity measurements at different shear rates showed that all the paraffin-based samples have a Newtonian behaviour, but for the paraffin with nanoclay particles.[34] Therefore, the viscosity of the paraffin with polymer does not depend on the shear rate. Consequently, for these viscosity measurements, it was decided to take a constant shear rate of 200 1/s and to vary only the temperature. The measurements of

DOI: 10.13009/EUCASS2017-159

the viscosity of the samples at different temperatures are shown in Fig. 7. It can be noticed that the viscosity increases with increasing polymer addiction. Moreover, with increasing temperature, the viscosities of the three blends tend to decrease faster than that of pure paraffin. This is due to the polymer decomposition.

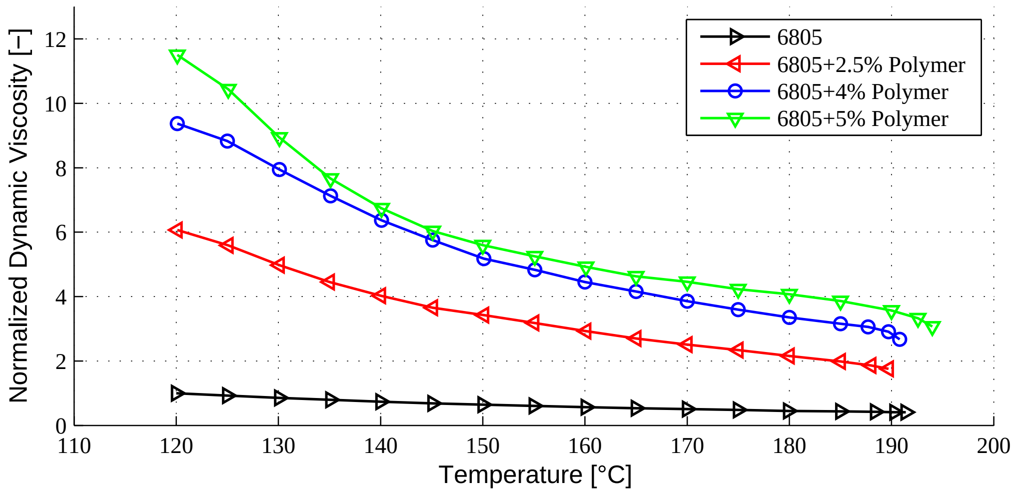

Figure 7: Viscosity of paraffin 6805 with different additives at a constant shear rate

5. Results and Discussion

In this paper, the influence of the fuel composition and configuration on the entrainment process is discussed. Therefore, in these test campaigns, all the combustion tests were performed at a constant oxidizer mass flow of 50 g/s. Four different paraffin-based fuels and three different fuel slab configurations were tested. By analysing the PSD results of POD and ICA, it is possible to obtain the most excited frequencies and wavelengths for each of them. POD enables the recognition of the main energetic structures of the flow field, ICA identifies the leading independent structures underlying the data. The analysis was carried out on 1 second (10000 frames) during the steady-state. Frequency and wavelength peaks were taken for each fuel formulations and configurations and then compared.

The results show that the combustion is dominated by wave-like structures for all the fuels and that the most excited frequencies and wavelengths characterizing the liquid melt layer depend on the fuel geometry and viscosity.

5.1 Fuel Configuration

An investigation on the influence of the fuel configuration on the waves instability mechanism was necessary at the beginning of the research. In fact, in each combustion tests a whole range of different frequencies and wavelengths is amplified: some of them are related to the KHI process (so to the entrainment process), some are connected to the vortex shedding caused by the fuel slab step and others just to random appearing vortices. In order to understand which frequencies and wavelengths are actually related to the entrainment process, it was necessary to perform a study on the influence of the fuel step on the combustion mechanism. In this way, it was possible to recognize all the frequencies related to the presence of the step. For what concerns random appearing vortices, a comparison between the POD and ICA results was performed: if a frequency peak appears only in the POD, it is most likely related to a random energetic vortex. On the other hand, if a frequency peak appears only in the ICA, it is most likely a periodic but not energetic signal, so not important. Those peaks which appear in both POD and ICA are periodic and energetic signals, so related to the main events during the combustion process. Therefore, a combination of the two decomposition techniques is necessary in order to better characterize the dynamic of the process.

DOI: 10.13009/EUCASS2017-159

In this test campaign all the combustion tests were performed with the fuel composition 6805 with 5% polymer and oxidizer mass flow of 50 g/s. Fuel slabs with 5°, 20°and 90°forward-facing ramp (FFR) were investigated.
The combustion of the fuel slab with 5°forward-facing ramp is characterized by a poor flame holding. A wave-like structure can be seen but points of local extinction of the flame can be detected along the fuel surface as the flame is developing. The flame appears to be not even and made up of elongated filaments, see Fig. 8. Two ranges of frequencies are excited with this configuration: 170-190 Hz and 300-340 Hz. The lower frequency range is related to the vortex shedding at the beginning of the ramp (VS1).

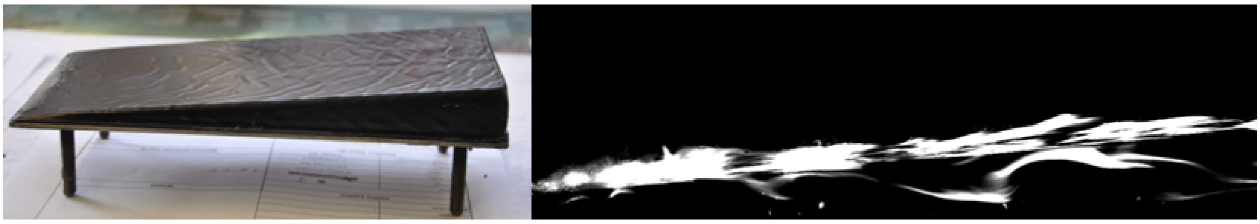

Figure 8: Fuel slab and combustion flame with 5°FFR

A proper flame holding is reached in the fuel configuration with the 20°FFR. The recirculation zone creates large waves and flame front at the head of the fuel slab. The flame is burning continuously along the fuel surface with no points of local extinction, see Fig. 9. This coherent and regular wave-like structure is related to the vortex shedding at the end of the ramp. Three amplified frequency ranges can be detected with this configuration: 200-230 Hz, 300-340 Hz and 400-500 Hz. The first and the last range are related respectively to the vortex shedding produced at the beginning (VS1) and at the end of the ramp (VS2).

Figure 9: Fuel slab and combustion flame with 20°FFR

In the configuration with the 90°forward-facing step (FFS) a big flow separation and recirculation zone is visible just after the step. The separation region experiences a weak regular vortex shedding which leads to accumulation of vorticity within the recirculation zone. This makes the region grow in size until a large scale vortex is ejected from the recirculation zone, with a consequent reduction in recirculation region size and reattachment length. The vorticity accumulation process induces a low frequency flapping of the shear layer and, consequently, a fluctuation of the reattachment point within a "reattachment zone"[48] (see Fig. 11). In this configuration, three excited frequency ranges were found: 90-120 Hz, 320-330 Hz and 400-450 Hz. The first range is related to the low frequency flapping motion of the shear layer. The last range is linked to the vortex shedding produced at the end of the step (VS2).

Figure 10: Fuel slab and combustion flame with 90°FFS

DOI: 10.13009/EUCASS2017-159

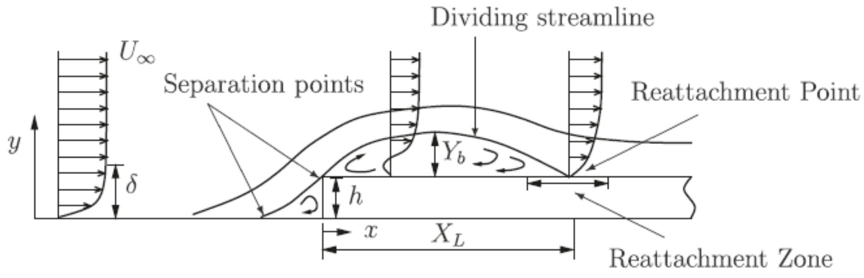

Figure 11: Flow field over a FFS, taken from Sherry et al.[48]

The experimental vortex shedding frequencies were also compared with the theoretical ones, according to the formula taken from Carmicino at al.[6] for the vortex shedding at the inlet of the fuel grain:

$$f_{VS} = Sr\frac{4}{\pi}\frac{\dot{m}_{Ox}}{D^3}\frac{R_{ox}T_{ox}}{p} \tag{1}$$

Here, Sr is the Strouhal number, $\dot{m}_{ox}$ is the oxidizer mass flow, D is the characteristic length, i. e. the port diameter in the case of a fuel grain, R_{ox} is the oxidizer gas constant, T_{ox} is the oxidizer temperature and p is the combustion chamber pressure.
This formula can be adapted to the single fuel slab configuration:

$$f_{VS} = Sr\frac{4}{\pi}\frac{\dot{m}_{Ox}}{D^3}\frac{R_{ox}T_{ox}}{p} = Sr\frac{G_{Ox}}{D}\frac{R_{ox}T_{ox}}{p} \tag{2}$$

where G_{Ox} is the oxidizer mass flux. For what concerns the Strouhal number, it mostly depends on the fluid dynamic characteristics of the velocity profile at the step. However, a Strouhal number varying in the range $0.25 < Sr < 0.5$ can be found in literature for the velocity fluctuations at the end of the jet core.[6]

The theoretical vortex shedding frequencies were all in the range 150-220 Hz for VS1 (vortices at the beginning of the ramp) and in the range 400-550 Hz for VS2 (vortices at the end of the ramp). These results match really good with the frequencies which were found experimentally from the combustion tests.

At the end of this study, it was possible to state that the frequencies related to the KHI are those in the range 300-340 Hz for the investigated fuel formulation and oxidizer mass flow. In the same way it was also possible to identify the longitudinal wavelengths connected to the instability mechanism. A summary of the results of the dependency of frequencies and wavelengths from the fuel configuration can be seen in Table 1. It has to be underlined that all these frequency and wavelength values were found both in POD and ICA results, so they are all connected to energetic and periodic structures. The only values that appeared only in the POD results are those connected to the VS2 in the configuration with 90°FFS. This means that those vortices bring a lot of energy in the flow field but they do not appear periodically. This is due to the fact that the recirculation zone on the step disturbs the periodicity of the vortex shedding.

DOI: 10.13009/EUCASS2017-159

Table 1: Amplified frequencies and wavelengths from POD and ICA for 6805+5%polymer and $\dot{m}_{Ox} = 50g/s$

	Flap	**VS1**	**KHI**	**VS2**
5°FFR	-	170-190 Hz	300-340 Hz	-
	-	3.3-5 mm	2.5-3.5 mm	-
20°FFR	-	200-230 Hz	300-340 Hz	400-500 Hz
	-	3.7-5 mm	2.5-3.3 mm	1.4-2 mm
90°FFS	90-120 Hz	-	320-330 Hz	400-450 Hz (POD)
	5-7 mm	-	2.7-2.9 mm	2-2.5 mm (POD)

5.2 Fuel Viscosity

After having identified the frequencies connected with the KHI for a particular fuel formulation, it was possible to study the influence of the fuel viscosity on the entrainment mechanism, independently from the fuel configuration.

In this test campaign, all the combustion tests were performed with the fuel configuration with the 20°FFR and oxidizer mass flow of 50 g/s. With this fuel slab a good flame holding and a continuous flame front is obtained (see Sec. 5.1), which means a better quality of the video analysis. Moreover, the recirculation zone is limited in size. Lower FFR angles have smaller recirculation regions but, consequently, do not guarantee a good flame attachment to the fuel slab surface; on the other hand with higher angles the recirculation zone is becoming bigger and a separation region could appear. Four different fuel formulations were investigated (see Sec. 4) and a dependence of the excited frequencies and wavelengths on the fuel viscosity was found.

The frequency peaks connected to the KHI are all in the low and/or medium frequency range (<600 Hz) for the investigated fuel formulations and their values become lower as the viscosity increases. The longitudinal wavelengths show peaks in the range 1.8-3.5 mm. This is in the range of the critical and most amplified waves predicted by the Kelvin-Helmholtz instability theory.[15,37] The higher the fuel viscosity, the higher the values of the most excited wavelengths are. So, the amplified frequency and wavelength values are influenced by the liquid viscosity, as expected from the entrainment[24,25] and Kelvin-Helmholtz[15] theories. In particular, by increasing the viscosity, the frequency values decrease and the longitudinal wavelengths increase, see Fig. 12 and 13. This means that the higher the viscosity, the more stable the liquid layer is. This leads to a lower number of released and, consequently, entrained droplets and, thus, to a lower regression rate.

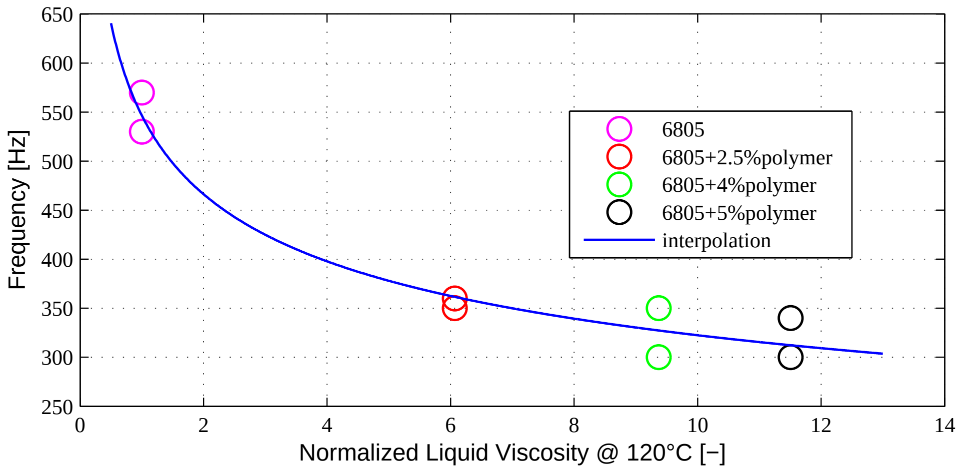

Figure 12: Dependency of the KHI frequencies on the fuel viscosity ($\dot{m}_{Ox} = 50g/s$)

DOI: 10.13009/EUCASS2017-159

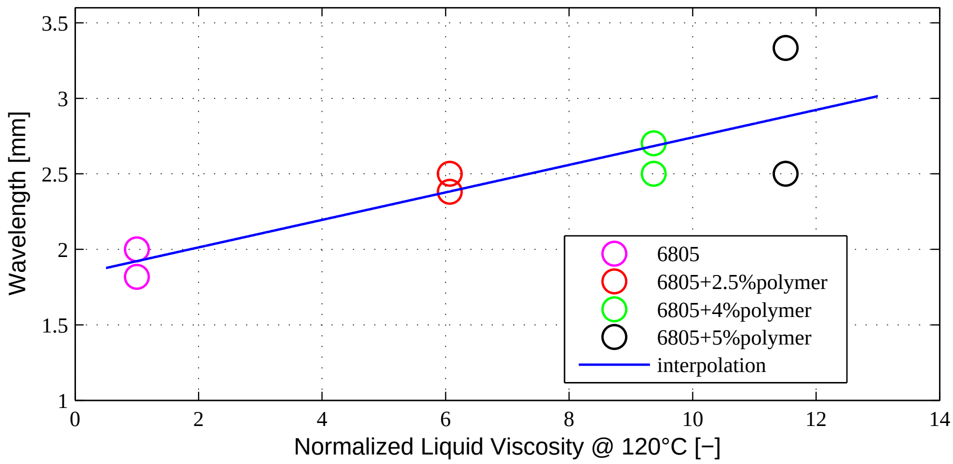

Figure 13: Dependency of the KHI longitudinal wavelengths on the fuel viscosity ($\dot{m}_{Ox} = 50g/s$)

6. Conclusion

The combustion behaviour of different paraffin 2D fuel slab samples burning with GOX was investigated with an optical combustion chamber. High speed video imaging enabled the collection of a huge amount of data, which needs to be analysed in detail. Therefore, two automated data evaluation techniques based on POD and ICA were applied to the analysis of the luminosity field of images in a reactive flow. This allows for an analysis of the considered scalar field by identifying leading components during the burning process. POD and ICA were applied separately to the same luminosity data.

In this work, the influence of the fuel configuration and formulation on the liquid layer instability process has been investigated. In particular, the dependence of amplified frequencies and wavelengths on the angled front step has been investigated. The combustion tests have been performed with the fuel composition 6805 with 5% polymer and an oxidizer mass flow of 50 g/s. Fuel slabs with 5°, 20°and 90°forward-facing ramp (FFR) have been investigated. From the results it is possible to notice that different frequency and wavelength ranges are excited from different slab angles. Some of them are related to the vortex shedding produced at the beginning (VS1) and/or at the end (VS2) of the ramp, some to the flapping motion of the shear layer caused by the ejection of a large scale vortex from the recirculation region. Others are connected to the KHI, so to the liquid layer instability mechanism. After having identified the frequencies connected with the KHI for a particular fuel formulation, it was possible to study the influence of the fuel viscosity on the entrainment mechanism, independently from the fuel configuration. A dependency of the most amplified frequencies and wavelengths on the fuel liquid viscosity has been found. In particular, the higher is the viscosity the lower are the values of the excited frequencies and the longer are the longitudinal waves.

Concluding, it was shown that the combustion of paraffin-based hybrid rocket fuels is dominated by wave-like structures and that the most excited frequencies and wavelengths characterizing the liquid melt layer depend on the fuel viscosity and geometry. This is important to better understand the onset of the entrainment process, which is connected to the amplification of longitudinal unstable waves caused by the high velocity gas flow over the fuel surface.

This is the first time and a novelty that POD and ICA were applied to image data collected in an optically accessible combustion chamber in order to evaluate combustion phenomena in hybrid rocket fuels. The results obtained prove the robustness of the two decomposition methods and the effectiveness of the video analysis process. Nevertheless, some limitations have to be taken into account when the results are analysed. First of all, the analysis is performed on 2D images. This means that what we analysed can be the superposition of all the combustion phenomena appearing on the fuel surface along the whole width. Furthermore, the waves on the fuel surface do not probably move straight in the horizontal direction. Moreover, the brightness of the flame and the condensed products which polluted the window increase the complexity of the optical measurement. Finally, it has to be highlighted that at the base of the whole analysis there is the assumption that the flame front follows the liquid layer. This is the reason why it is assumed that the waves appearing on the flame correspond to the waves of the liquid layer.

DOI: 10.13009/EUCASS2017-159

Acknowledgements

This work was partially funded by the DLR project ATEK (Antriebstechnologien und Komponenten fuer Traegersysteme: Propulsion Technologies and Components for Launcher Systems). The support of the M11 team and the propellants department is greatly acknowledged.

References

[1] R. S. Amano, Yi-Hsin Yen, Timothy C. Miller, Adam Ebnit, Malissa Lightfoot, and Venke Sankaran. Study of the liquid breakup process in solid rocket motor. *Journal of Spacecraft and Rockets*, 53(5):980–992, September 2016.

[2] K. Bizon, G. Continillo, S. Lombardi, E. Mancaruso, and B.M. Vaglieco. Spatial and temporal independent component analysis of flame dynamics in diesel engine. In *XXXVI Meeting of the Italian Section of the Combustion Institute*, June 2013.

[3] K. Bizon, G. Continillo, E. Mancaruso, S.S. Merola, and B.M. Vaglieco. Pod-based analysis of combustion images in optically accessible engines. *Combustion and Flame*, 157(4):632–640, April 2010.

[4] K. Bizon, S. Lombardi, G. Continillo, E. Mancaruso, and B. M. Vaglieco. Analysis of diesel engine combustion using imaging and independent component analysis. *Proceedings of the Combustion Institute*, 34(2):2921–2931, January 2013.

[5] A. Cammilleri, F. Gueniat, J. Carlier, L. Pastur, E. Memin, F. Lusseyran, and G. Artana. POD-spectral decomposition for fluid flow analysis and model reduction. *Theoretical and Computational Fluid Dynamics*, 27(6):787–815, February 2013.

[6] C. Carmicino. Acoustics, vortex shedding, and low-frequency dynamics interaction in an unstable hybrid rocket. *Journal of Propulsion and Power*, 25(6):1322–1335, November 2009.

[7] P. Carrick and C. Larson. Lab scale test and evaluation of cryogenic solid hybrid rocket fuels. In *31st Joint Propulsion Conference and Exhibit*. American Institute of Aeronautics and Astronautics, July 1995.

[8] Ashley A. Chandler, Elizabeth T. Jens, Brian J. Cantwell, and G. Scott Hubbard. Visualization of the liquid layer combustion of paraffin fuel at elevated pressures. In *63rd International Astronautical Congress*, 2012.

[9] Ashley A. Chandler, Elizabeth T. Jens, Brian J. Cantwell, and G. Scott Hubbard. Visualization of the liquid layer combustion of paraffin fuel for hybrid rocket applications. In *48th AIAA/ASME/SAE/ASEE Joint Propulsion Conference and Exhibit*. American Institute of Aeronautics and Astronautics, July 2012.

[10] Anindya Chatterjee. *An introduction to the proper orthogonal decomposition*, 2000.

[11] Martin Chiaverini. Review of solid-fuel regression rate behavior in classical and nonclassical hybrid rocket motors. In *Fundamentals of Hybrid Rocket Combustion and Propulsion*, pages 37–126. American Institute of Aeronautics and Astronautics, January 2007.

[12] H. K. Ciezki, J. Sender, W. Clau-oslash, A. Feinauer, and A. Thumann. Combustion of solid-fuel slabs containing boron particles in step combustor. *Journal of Propulsion and Power*, 19(6):1180–1191, November 2003.

[13] L. T. DeLuca, L. Galfetti, F. Maggi, G. Colombo, C. Paravan, A. Reina, P. Tadini, A. Sossi, and E. Duranti. An optical time-resolved technique of solid fuels burning for hybrid rocket propulsion. In *47th AIAA/ASME/SAE/ASEE Joint Propulsion Conference and Exhibit*. American Institute of Aeronautics and Astronautics, July 2011.

[14] S. Dodel, J. M. Herrmann, and T. Geisel. Comparison of temporal and spatial ica in fmri data analysis. *Proceedings of ICA 2000*, 2000.

[15] T. Funada and D. D. Joseph. Viscous potential flow analysis of kelvin-helmholtz instability in a channel. *Journal of Fluid Mechanics*, 445, October 2001.

[16] A. Hyvarinen. One-unit contrast functions for independent component analysis: a statistical analysis. *Neural Networks for Signal Processing VII. Proceedings of the 1997 IEEE Workshop*, 1997.

DOI: 10.13009/EUCASS2017-159

[17] A. Hyvarinen and E. Oja. Independent component analysis: algorithms and applications. *Neural Networks*, 13(4-5):411–430, June 2000.

[18] Elizabeth T. Jens, Ashley A. Chandler, Brian Cantwell, G. Scott Hubbard, and Flora Mechentel. Combustion visualization of paraffin-based hybrid rocket fuel at elevated pressures. In *50th AIAA/ASME/SAE/ASEE Joint Propulsion Conference*. American Institute of Aeronautics and Astronautics, July 2014.

[19] Elizabeth T. Jens, Victor A. Miller, and Brian J. Cantwell. Schlieren and oh* chemiluminescence imaging of combustion in a turbulent boundary layer over a solid fuel. *Experiments in Fluids*, 57(3), February 2016.

[20] Elizabeth T. Jens, Victor A. Miller, Flora S. Mechentel, Brian J. Cantwell, and Scott Hubbard. A visual study of the combustion of high-regression rate and classical hybrid rocket fuels. In *51st AIAA/SAE/ASEE Joint Propulsion Conference*. American Institute of Aeronautics and Astronautics, July 2015.

[21] Elizabeth T. Jens, Pavan Narsai, Brian Cantwell, and G. Scott Hubbard. Schlieren imaging of the combustion of classical and high regression rate hybrid rocket fuels. In *50th AIAA/ASME/SAE/ASEE Joint Propulsion Conference*. American Institute of Aeronautics and Astronautics, July 2014.

[22] A. Karabeyoglu. Hybrid rocket propulsion for future space launch. In *Aero/Astro 50th Year Anniversary Stanford University*, 2008.

[23] A. Karabeyoglu, D. Altman, and D. Bershader. *Transient combustion in hybrid rockets*. PhD thesis, Standford University, jul 1995.

[24] A. Karabeyoglu, D. Altman, and B. J. Cantwell. Combustion of liquefying hybrid propellants: Part 1, general theory. *Journal of Propulsion and Power*, Vol.18(No. 3):610–620, May 2002.

[25] A. Karabeyoglu and B. J. Cantwell. Combustion of liquefying hybrid propellants: Part 2, stability of liquid films. *Journal of Propulsion and Power*, Vol. 18(No. 3):621–630, May 2002.

[26] A. Karabeyoglu, B.J. Cantwell, and D. Altman. Development and testing of paraffin-based hybrid rocket fuels. In *37th AIAA/ASME/SAE/ASEE Joint Propulsion Conference and Exhibit*, Salt Lake City, Utah, July 2001. American Institute of Aeronautics and Astronautics.

[27] A. Karabeyoglu, Brian J. Cantwell, and Jose Stevens. Evaluation of homologous series of normal-alkanes as hybrid rocket fuels. In *41st AIAA/ASME/ASEE Joint Propulsion Conference*, July 2005.

[28] A. Karabeyoglu, J. Stevens, D. Geyzel, B. Cantwell, and D. Micheletti. High performance hybrid upper stage motor. In *47th AIAA/ASME/SAE/ASEE Joint Propulsion Conference and Exhibit*. American Institute of Aeronautics and Astronautics, July 2011.

[29] A. Karabeyoglu, G. Zilliac, B. J. Cantwell, S. DeZilwa, and P. Castellucci. Scale-up tests of high regression rate paraffin-based hybrid rocket fuels. *Journal of Propulsion and Power*, 2004(6), November 2004.

[30] Gaetan Kerschen, Jean claude Golinval, Alexander F. Vakakis, and Lawrence A. Bergman. The method of proper orthogonal decomposition for dynamical characterization and order reduction of mechanical systems: An overview. *Nonlinear Dynamics*, 41(1-3):147–169, August 2005.

[31] M. Kobald, H. K. Ciezki, and S. Schlechtriem. Optical investigation of the combustion process in paraffin-based hybrid rocket fuels. In *49th AIAA/ASME/SAE/ASEE Joint Propulsion Conference*. American Institute of Aeronautics and Astronautics, July 2013.

[32] M. Kobald, A. Petrarolo, and S. Schlechtriem. Combustion visualization and characterization of liquefying hybrid rocket fuels. In *51st AIAA/SAE/ASEE Joint Propulsion Conference*. American Institute of Aeronautics and Astronautics, July 2015.

[33] M. Kobald and S. Schlechtriem. Investigation of different hybrid rocket fuels in a 2d slab burner with optical techniques. In *Tenth International Conference on Flow Dynamics*, 2013.

[34] M. Kobald, C. Schmierer, H. K. Ciezki, S. Schlechtriem, E. Toson, and L. T. De Luca. Viscosity and regression rate of liquefying hybrid rocket fuels. *Journal of Propulsion and Power*, pages 1–7, March 2017.

DOI: 10.13009/EUCASS2017-159

[35] M. Kobald and E. Toson. Evaluation of paraffin-based fuels for hybrid rocket engines. In *50th AIAA/ASME/SAE/ASEE Joint Propulsion Conference*. American Institute of Aeronautics and Astronautics, July 2014.

[36] M. Kobald, E. Toson, H. Ciezki, S. Schlechtriem, S. di Betta, M. Coppola, and L. De Luca. Rheological, optical and ballistic investigations of paraffin-based fuels for hybrid rocket propulsion using a 2d slab-burner. In *5TH EUROPEAN CONFERENCE FOR AERONAUTICS AND SPACE SCIENCES (EUCASS)*, 2013.

[37] M. Kobald, I. Verri, and S. Schlechtriem. Theoretical and experimental analysis of liquid layer instability in hybrid rocket engines. *CEAS Space Journal*, 7(1):11–22, January 2015.

[38] C. Larson, M. DeRose, K. Pfeil, P. Carrick, M. DeRose, K. Pfeil, P. Carrick, and C. Larson. Tube burner studies of cryogenic solid combustion. In *33rd Joint Propulsion Conference and Exhibit*. American Institute of Aeronautics and Astronautics, July 1997.

[39] C. Larson, K. Pfeil, M. DeRose, and P. Garrick. High pressure combustion of cryogenic solid fuels for hybrid rockets. In *32nd Joint Propulsion Conference and Exhibit*. American Institute of Aeronautics and Astronautics, July 1996.

[40] John J. Marano and Gerald D. Holder. A general equation for correlating the thermophysical properties of n-paraffins, n-olefins, and other homologous series. 3. asymptotic behavior correlations for thermal and transport properties. *Industrial and Engineering Chemistry Research*, 36(6):2399–2408, June 1997.

[41] John J. Marano and Gerald D. Holder. General equation for correlating the thermophysical properties ofn-paraffins,n-olefins, and other homologous series. 1. formalism for developing asymptotic behavior correlations. *Industrial and Engineering Chemistry Research*, 36(5):1887–1894, May 1997.

[42] John J. Marano and Gerald D. Holder. General equation for correlating the thermophysical properties ofn-paraffins,n-olefins, and other homologous series. 2. asymptotic behavior correlations for pvt properties. *Industrial and Engineering Chemistry Research*, 36(5):1895–1907, May 1997.

[43] G. Marxman and M. Gilbert. Turbulent boundary layer combustion in the hybrid rocket. In *9th Symposium (International) on Combustion*, pages 371–383. Elsevier, 1963.

[44] Ichiro Nakagawa and Satoshi Hikone. Study on the regression rate of paraffin-based hybrid rocket fuels. *Journal of Propulsion and Power*, Vol.27(No.6):1276–1279, November 2011.

[45] Nicolas Pelletier. *Etude des Phenomenes de Combustion dans un Propulseur Hybride. Modelisation et Analyse Experimentale de la Regression des Combustibles Liquefiables*. PhD thesis, Institut Superieur de L'Aeronatique et de L'Espace, Toulouse, 2009.

[46] A. Petrarolo and M. Kobald. Evaluation techniques for optical analysis of hybrid rocket propulsion. *Journal of Fluid Science and Technology*, 11(4):JFST0028–JFST0028, 2016.

[47] A. Petrarolo, M. Kobald, and S. Schlechtriem. Optical analysis of hybrid rocket combustion with decomposition methods. In *Space Propulsion Conference*, May 2016.

[48] M. Sherry, D. Lo Jacono, and J. Sheridan. An experimental investigation of the recirculation zone formed downstream of a forward facingstep. *Journal of Wind Engineering and Industrial Aerodynamics*, 98(12):888–894, December 2010.

[49] James V. Stone. *Independent Component Analysis. A Tutorial Introduction,*. A Brandford Book, 2004.

[50] Hiroshi Tada, Shigeru Aso, Yasuhiro Tani, Sho Oyama, Kentaro Araki, and Toru Shimada. Visualization of flames in combustion chamber of hybrid rocket engine with multi-section swirl injection method. In *50th AIAA/ASME/SAE/ASEE Joint Propulsion Conference*. American Institute of Aeronautics and Astronautics, July 2014.

[51] Yutaka Wada, You Kawabata, Tomonori Itagaki, Keisuke Seki, Ryuichi Kato, Nobuji Kato, and Keiichi Hori. Observation of combustion behavior of low melting temperature fuel for hybrid rocket using double slab motor. In *10th International Symposium on Special Topics in Chemical Propulsion*, June 2014.

[52] G. Zilliac, B. S. Waxman, A. Karabeyoglu, B. Cantwell, and B. J. Evans. Peregrine hybrid rocket motor development. In *50th AIAA/ASME/SAE/ASEE Joint Propulsion Conference*. American Institute of Aeronautics and Astronautics, July 2014.

DOI: 10.13009/EUCASS2017-159

Abbreviations

DLR	Deutsches Zentrum für Luft- und Raumfahrt (German Aerospace Center)
GOX	Gaseous Oxygen
HRE	Hybrid Rocket Engines
HDPE	High-density Polyethylene
HTPB	Hydroxyl-terminated Polybutadien
PMMA	PolyMethyl MethAcrylate
KHI	Kelvin-Helmholtz Instability
PCA	Principal Component Analysis
POD	Proper Orthogonal Decomposition
SVD	Singular Value Decomposition
NIPALS	Nonlinear Iterative Partial Least Square
PSD	Power Spectral Density
(s/t)ICA	(spatial/temporal) Independent Component Analysis
FFR	Forward Facing Ramp
FFS	Forward Facing Step
VS1	Vortex shedding at the beginning of the fuel ramp
VS2	Vortex shedding at the end of the fuel ramp

Nomenclature

f_{VS}	vortex shedding frequency $[Hz]$
Sr	Strouhal number
$\dot{m}_{ox}$	oxidizer mass flow $[kg/s]$
D	characteristic length $[m]$
R_{ox}	oxidizer gas constant $[J/(kgK)]$
T_{ox}	oxidizer temperature $[K]$
p	combustion chamber pressure $[Pa]$
G_{Ox}	oxidizer mass flux $[kg/(m^2 s)]$